

Sebetralstat (KVD900): A Potent and Selective Small Molecule Plasma Kallikrein Inhibitor Featuring a Novel P1 Group as a Potential Oral On-Demand Treatment for Hereditary Angioedema

Rebecca L. Davie,* Hannah J. Edwards, D. Michael Evans, Simon T. Hodgson, Michael J. Stocks, Alun J. Smith, Louise J. Rushbrooke, Stephen J. Pethen, Michael B. Roe, David E. Clark, Paul A. McEwan, and Sally L. Hampton



Cite This: <https://doi.org/10.1021/acs.jmedchem.2c00921>



Read Online

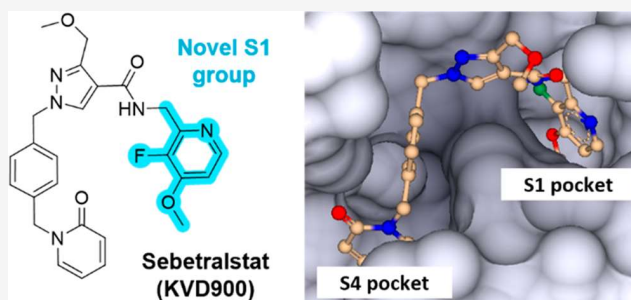
ACCESS |

Metrics & More

Article Recommendations

Supporting Information

ABSTRACT: Hereditary angioedema (HAE) is a rare genetic disorder in which patients experience sudden onset of swelling in various locations of the body. HAE is associated with uncontrolled plasma kallikrein (PKa) enzyme activity and generation of the potent inflammatory mediator, bradykinin, resulting in episodic attacks of angioedema. Herein, we disclose the discovery and optimization of novel small molecule PKa inhibitors. Starting from molecules containing highly basic P1 groups, which typically bind to an aspartic acid residue (Asp189) in the serine protease S1 pocket, we identified novel P1 binding groups likely to have greater potential for oral-drug-like properties. The optimization of P4 and the central core together with the particularly favorable properties of 3-fluoro-4-methoxypyridine P1 led to the development of sebetralstat, a potent, selective, orally bioavailable PKa inhibitor in phase 3 for on-demand treatment of HAE attacks.



INTRODUCTION

Hereditary angioedema (HAE) is a rare genetic disease in which patients experience painful swelling in various locations of the body, which can be life-threatening when occurring in the upper airway. HAE attacks are associated with uncontrolled plasma kallikrein (PKa) activity and generation of bradykinin (BK). Ecallantide, an injectable PKa inhibitor, was shown to be highly effective in treating HAE attacks and demonstrated the critical role of PKa.¹ C1 inhibitor (C1-INH) is the primary physiological inhibitor of PKa. C1-INH deficiency caused by mutations in the *SERPINC1* gene are responsible for the most common forms of HAE. HAE associated with a low level of C1-INH and with dysfunctional forms of C1-INH is categorized as HAE type I and HAE type II, respectively.^{2,3} The estimated prevalence for HAE is approximately 1 in 50 000 people.⁴ HAE can also occur in the presence of normal C1-INH activity, and PKa has been implicated in causing attacks in people with normal C1-INH HAE.⁵

PKa is derived from its zymogen, plasma prekallikrein, which circulates in the blood. Plasma prekallikrein is activated by factor (F) XIIa to form PKa, which then forms a feedback loop driving the conversion of FXII to its active form, FXIIa. The physiological actions of PKa associated with HAE have been primarily attributed to its capacity to cleave high-molecular-weight kininogen (HK) to generate the nine amino acid peptide hormone BK. The kallikrein–kinin system, shown in

Figure 1, is regulated by C1-INH, an important inhibitor of both PKa and FXIIa. Inhibition of PKa is an established therapy for HAE and has been implicated as a treatment for other diseases including, for example, diabetic macular edema and SARS-CoV-2.^{6,7}

The active site of PKa comprises multiple subsites described using the nomenclature of Schechter and Berger (e.g., S1, S2, etc. for subsites and P1, P2, etc. for groups of the ligand that occupy the corresponding subsites).⁸ PKa belongs to the trypsin-like serine protease family; the specificity for this family of proteases for positively charged amino acids such as lysine or arginine is driven by an aspartic acid residue (Asp189) situated at the base of the S1 pocket that forms a strong interaction with the positively charged amino acids. Development of orally bioavailable small molecule inhibitors of PKa has proved challenging because the positively charged basic P1 groups that were believed to be required for high levels of potency are often detrimental to oral bioavailability.⁹ This is illustrated by the relatively few PKa inhibitors that have

Received: June 10, 2022

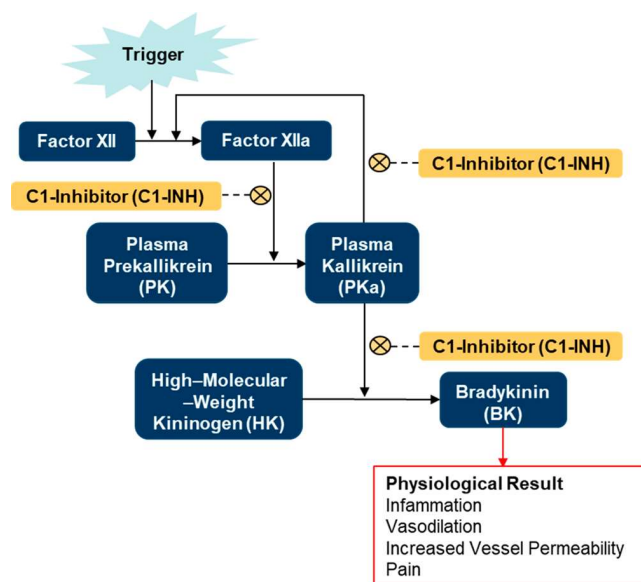


Figure 1. Activation of the kallikrein–kinin system. Activation is indicated by black solid arrows, and inhibition is indicated by dashed lines.

reached clinical development (Figure 2) despite the plethora of small molecule PKa inhibitor patents published by numerous organizations.¹⁰

Lowering the basicity of the P1 group has been a strategy successfully used to identify orally bioavailable inhibitors of other trypsin-like serine proteases such as thrombin, FXa, and FXIa. For this reason, our aim was to identify a new class of PKa inhibitor that contained a P1 group that was not charged at physiological pH to increase the likelihood of attaining favorable oral-drug-like properties. Taking inspiration from highly ligand efficient, strongly basic benzamidine PKa inhibitors **1** and **2** (calculated pK_a 11.6) reported in the literature,¹⁵ we systematically reduced the basicity of the P1 group, first to the benzylamine (calculated pK_a 9.1), then to the weakly basic aminoisoquinoline (calculated pK_a 7.5), and finally to the neutral P1 binders (calculated pK_a <6). Significant achievements during optimization are summarized in Figure 3, culminating in the discovery of sebetralstat (KVD900), a molecule that features a novel 3-fluoro-4-methoxypyridyl P1 group.

RESULTS AND DISCUSSION

Reducing the Basicity of the P1 Group. Compound **2** is a potent PKa inhibitor (IC_{50} 62 nM); however, it lacks oral bioavailability, as demonstrated by a prodrug approach having been investigated.¹⁶ Compounds containing highly polar charged groups tend to suffer from poor passive permeability that impacts oral absorption and hinders development of oral drugs. The potency and ligand efficient nature of compound **1** presented an ideal starting point to investigate P1 motifs of a reduced basic nature with favorable properties toward development of an oral drug. A variety of less basic P1 group motifs were installed onto the benzylpyrrole amide scaffold. However, only compound **3**, with a moderately basic benzylamine P1 group (calculated pK_a 9.1), was identified as sufficiently potent to warrant further optimization. This was pursued with the aim of identifying favorable alternative contacts within other pockets of the PKa active site that could compensate for the weaker salt bridge interaction provided by the amine (compared with an amidine) with Asp189 in the S1 pocket.

Exploring the S4 Pocket. P4 groups attached to the pyrrole core were explored based on literature protease S4 binders^{17–19} in combination with probing the size and length of the S4 pocket (highlights of the SARs are shown in Table 1). The phenyl ring in **3** could be replaced with other heterocycles such as thiophene **8** and the PKa potency would be maintained. Investigations into the optimum length of the linker between the pyrrole and the phenyl ring revealed a preference for four methylene linkers (**9c**) and provided a 4-fold improvement in potency. With the use of this information, a series of biaryl substituents was synthesized looking at combinations of five- and six-membered aryl rings **9e–9n** and **4**. A total of three P4 substituents, phenylthiazole **9h**, benzylpyrazole **9n**, and benzylpyridone **4**, all showed further improvements in potency with PKa IC_{50} values of 72, 65, and 110 nM, respectively.

Taking the most active compounds **9h**, **9n**, and **4** and replacing the pyrrole ring with a pyrazole ring afforded a 6-fold increase in potency for **11** and even greater increase for **5** (Table 2). Interestingly, the phenylthiazole P4 group of **9h** did not show the same improvement in potency with the pyrazole core **10**. Additional five- and six-membered core rings were investigated, but the pyrazole ring appeared optimal for potency. With an optimized scaffold, we were then able to identify alternative P1 groups. Changing the benzylamine P1 group to a 1-aminoisoquinoline P1 group achieved further potency advances in both **12** (benzylpyrazole P4 group) and **6**

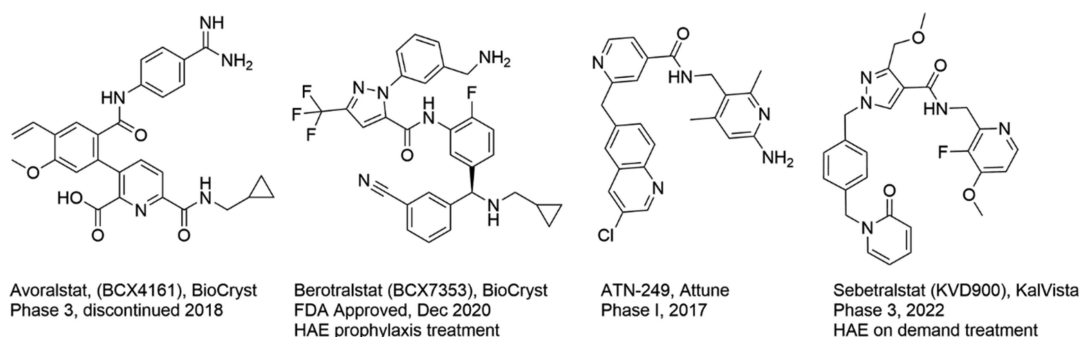


Figure 2. Oral small molecule PKa inhibitors with disclosed structures (avoralstat,¹¹ berotralstat,¹² ATN-249,^{13,14} sebetralstat) that have entered clinical trials.

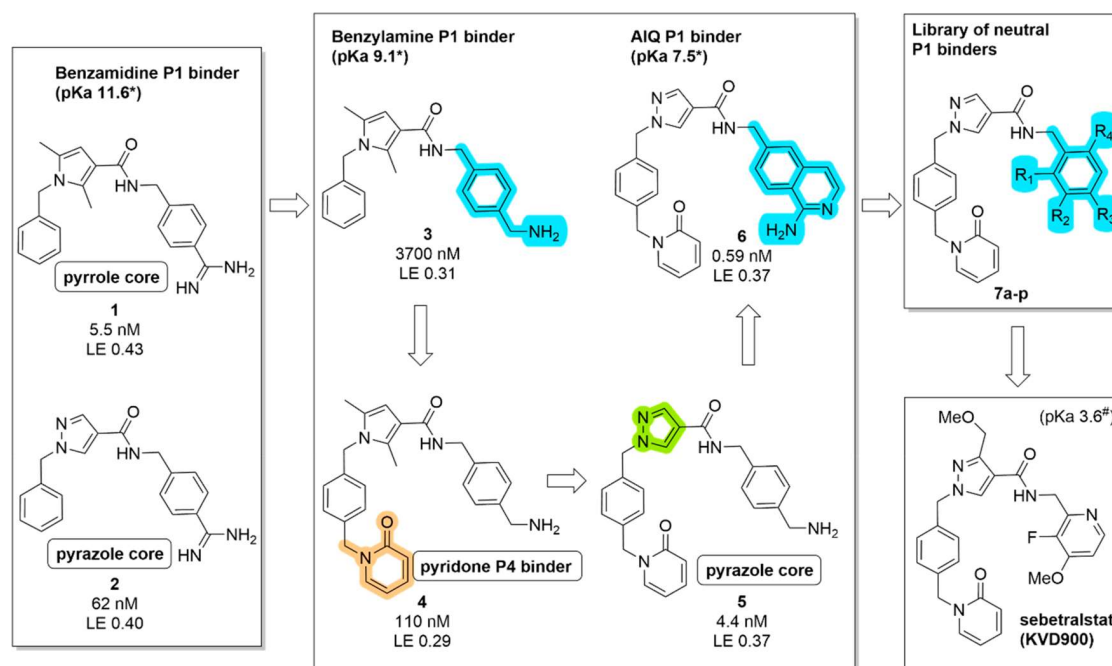


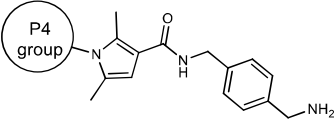
Figure 3. Evolution of our PKa inhibitors resulting in a highly potent scaffold (**6**) that inspired the design of a neutral P1 library. All PKa IC₅₀ values reported were performed in-house and are the mean values of two or more independent assays. pK_a values denoted with “*” are calculated values using ACD/Laboratories Percepta software (Toronto, ON, Canada). The pK_a denoted with “#” is a measured value from PION using a UV-metric method over the pH range 1.5–12.5.

(benzylpyridone P4 group) while also reducing basicity from a pK_a of 9.1 (calculated) with the benzylamine to a pK_a of 7.5 (calculated) with the 1-aminoisoquinoline (Table 3). Ligand efficiency (LE) was maintained, and improvements in lipophilic ligand efficiency (LLE)²⁰ were seen between matched pairs **11** and **12** and **5** and **6**. The benzylpyrazole analogue **12** suffered from a high turnover in human liver microsomes (HLM), while benzylpyridone **6** had more a moderate turnover but was poorly permeable in a 3 day Caco-2 permeability model. Despite these limitations, compounds **6** and **12** demonstrated the concept that potent PKa inhibitors could be achieved with a less basic P1 group when other parts of the compound bind efficiently.

Identification of Neutral P1 Groups. An extension of our strategy was to investigate the S1 pocket more widely with a range of neutral or weakly basic monocyclic P1 groups and potentially identify novel binding interactions. Compound **6** was selected over **12** as a starting point for further exploration based on its higher LLE and lower turnover in human liver microsomes; additionally, the synthetic ease and modular nature of the scaffold made it suitable for parallel synthesis. Hence, a library of amides was designed using the ZINC fragment-like database,²¹ initially selecting primary amines with MW < 250 and then filtering on physicochemical properties, shape-based overlays of known PKa P1 groups, and molecular docking experiments. This afforded a set of 140 amines. Reactions were performed in 96-well plates on a 0.0125 mmol scale; reactions were quenched with methanol and, after evaporation of the solvent, redissolved in DMSO at a fixed concentration. All compounds were screened without purification in the biochemical assay with a fluorogenic substrate to determine the ability to inhibit PKa activity. Prior to testing of the library plates, it was demonstrated that the carboxylic acid intermediate, methyl ester analogue (a

result of quenching with methanol), and a selection of the substituted benzylamine monomers from the library set did not possess any significant inhibitory activity up to 10 000 nM. Compounds were initially tested twice, each at single concentrations of 1000 and 100 nM, respectively. Compounds that showed a percentage of inhibition greater than 70% at 1000 nM and greater than 30% at 100 nM were screened in a dose–response mode for IC₅₀ determination. A cluster of substituted phenyl ring P1 groups was identified with PKa inhibition; a selection of the SARs are presented in Table 4 to highlight the effects of substituents and their positions on the percentage inhibition. Reference compound **7a**, with an unsubstituted phenyl ring, showed limited inhibition (<30%) at both 1000 and 100 nM. An interesting observation came from the analysis of the trends of the monosubstituted compounds. Of the monosubstituted compounds, the *m*-methoxy **7h** and *p*-methyl **7j** achieved inhibitions of greater than 30% at 100 nM, with IC₅₀ values of 90 and 88 nM and satisfying LEs of 0.31 and 0.32, respectively. Interestingly, an increase in potency was also observed with *ortho-ortho* disubstituted analogues **7l–7p** compared with analogous *ortho* monosubstituted examples **7b–7e**. Hence, the 2-fluoro-6-trimethylfluoro disubstituted analogue **7n** showed 83% inhibition at 100 nM and an IC₅₀ value of 7.8 nM, maintaining a ligand efficiency of 0.32. The nature of the substituent in these two *ortho* positions did not seem to have any significant effect. This SAR finding was difficult to rationalize prior to obtaining a crystal structure but seemed to indicate either a conformational preference for *ortho-ortho* substituted phenyl rings in the S1 pocket or synergistic effects between the substituents on the ring possibly intercepting different interactions in the S1 pocket. To check if these two SAR findings were additive, **13a** was prepared combining the 2,6-difluoro substitution with the 3-methoxy substituent. **13a**

Table 1. Exploration of the S4 Pocket for Potency



compd	P4 Group	PKa IC ₅₀ (nM)	compd	P4 Group	PKa IC ₅₀ (nM)
8		2700	9h		72
9a		>10,000	9i		480
9b		4800	9j		2700
9c		920	9k		5600
9d		3800	9l		730
9e		570	9m		580
9f		440	9n		65
9g		600	4		110

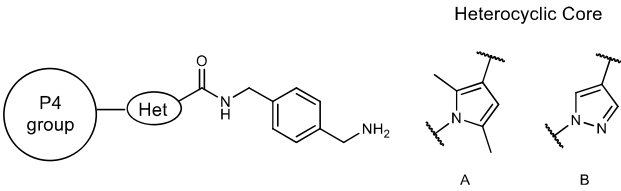
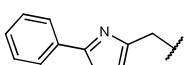
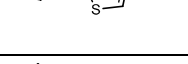
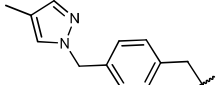
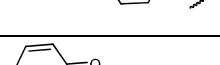
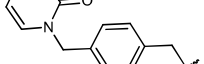

showed a further potency enhancement with an IC₅₀ value of 3.0 nM (Table 5). This breakthrough compound initiated the lead optimization program.

Lead Optimization of Compound 13a. A major advancement that contributed to the significant improvement of the ADME profile of this series involved the substitution of the central pyrazole ring. The unsubstituted pyrazole analogue, 13a, suffered from low Caco-2 permeability (3 day model); however, by incorporating substituents on the pyrazole ring, we were able to increase the permeability 5-fold with a methoxymethyl substituent, 13b. The improvement in permeability was maintained for a range of substituted pyrazoles, 13b–13f, 13j–13k, and 13m. We hypothesize that the observed increase in permeability of compounds with a pyrazole substituent is due to a combination of factors involving the ability of the substituent to mask the H-bond donor of the amide as well as an increase in the lipophilicity of the compounds. The methoxymethyl core pyrazole substituent 13b was favored, as it gave a similar potency to the unsubstituted pyrazole analogue 13a, and the impact on

HLM intrinsic clearance (CL_{int}), although high, was limited compared with those of the other pyrazole substituents tried (13c, 13e, and 13f). Modifications to the methoxy R₃ group, involving removal of the methyl to afford the hydroxy analogue 13g, replacement of the methyl group with a difluoromethyl group 13i, or exchanging the oxygen of the methoxy group with a carbon to afford the ethyl analogue 13h, were all detrimental to potency. The introduction of a pyrazole methoxymethyl substituent did not alter the trend observed for two *ortho* substituents; the removal of either fluorine at R₂ or R₄, 13d and 13l, respectively, negatively impacted potency. Alternative substituents to fluorine at both R₂ and R₄ were tolerated; a difluoromethyl group 13m at R₂ or a chlorine 13j or nitrile 13k at R₄ all afforded potent PKa inhibitors, with 13k being the most interesting, with an IC₅₀ value of 1.0 nM and promising ADME properties. Compounds 13b and 13k were progressed for further profiling.

With our newly identified neutral P1 groups comprising substituted phenyls, there was the potential for this class of compounds to have modest aqueous solubilities. The kinetic

Table 2. P4 and Core Modifications for PKa Potency Optimization

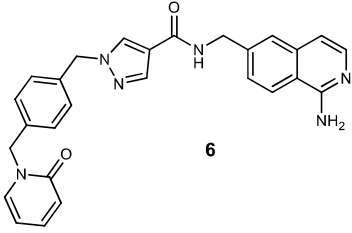
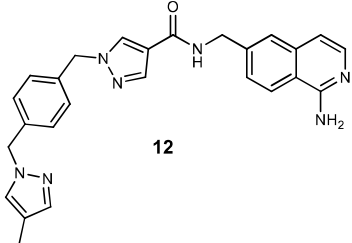
					
compd	P4 group	Het	PKa IC ₅₀ (nM)	LE	LLE
9h		A	72	0.32	3.4
10		B	850	0.29	3.7
9n		A	65	0.30	3.8
11		B	11	0.36	5.7
4		A	110	0.29	4.1
5		B	4.4	0.37	7.1

solubilities measured at the time did not reflect this and may indicate that the solubilities of neutral compounds from a solid physical form were underestimated when kinetic solubility prepared from a DMSO solution was used as a guide. Compounds **13b** and **13k** were further profiled in physiologically relevant thermodynamic solubility assays, and a solubility flag for these compounds was noted (Table 7). Thus, our second innovation toward oral inhibitors was to identify more

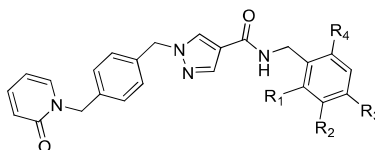
polar, but neutral (or weakly basic), heterocyclic P1 groups with increased solubilities over those of the phenyl P1 series.

Substituted heterocycles were screened (Table 6) and showed a range of PKa activities. Modest PKa potency was observed with five-membered rings, e.g., pyrazole and thiophene rings (**14h–14k**, IC₅₀ values 210–570 nM). In the case of six-membered rings, pyridines and pyrimidines were explored, affording a range of IC₅₀ values between 6.0 and 7900 nM. Pyridines with a nitrogen adjacent to the linker and a small 4-alkoxy substituent provided the most potent examples, with PKa IC₅₀ values of <10 nM (**14s**, **14w**, and **14x**). The isopropoxy analogue **14y** afforded a significantly less potent PKa inhibitor (2400 nM), suggesting a size limitation on this alkoxy group in the S1 pocket. Compounds **14s**, **14w**, and **14x** were progressed to ADME profiling (Table 7). Data from compounds **13b** and **13k** are also reported in Table 7 for comparative purposes. All compounds in Table 7 with the exception of **15** had acceptable permeabilities, with *P*_{app} values ranging from 9.0×10^{-6} cm/s for **14w** to 25×10^{-6} cm/s for **14s**. HLM CL_{int} values for this set appeared to follow a lipophilicity trend: **13b** with the highest cLogP (2.8) had the highest HLM CL_{int} of 92 μ L/min/mg of protein and **14w** with a cLogP of 1.8 had the lowest value of 14 μ L/min/mg of protein. Solubility assays were performed in physiologically relevant media to identify any potential solubility limitations. Compounds **14s** and **14w** were above the threshold of 0.1 mg/mL in FaSSIF and well above this threshold for fasted state simulated gastric fluid (FaSSGF). Both **14s** and **14w** were in a desirable LLE range for drug-like properties (LLE > 6, reduced lipophilicity), and this was reflected in improvements in both solubility and in vitro microsomal turnover values compared with the phenyl P1 containing compounds **13b** and **13k**. The pyrazole core substituent, R₁, was reinvestigated for the pyridyl P1 series by removing it altogether (**15**) or replacing it with other substituents: a trifluoromethyl group **16** and a cyclopropyl group **17**. Removing the substituent on the pyrazole

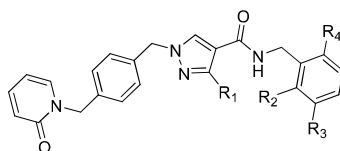
Table 3. Aminoisoquinoline P1 With Optimized Scaffolds^a

compd	PKa IC ₅₀ (nM)	LE	LLE	Caco-2 <i>P</i> _{app} ($\times 10^{-6}$ cm/s)	HLM CL _{int} (μ L/min/mg protein)
 6	0.59	0.37	7.2	2.0	37
 12	2.0	0.36	5.8	n.d.	181

^an.d., not determined.

Table 4. Selected SARs from the P1 Group Library^a

compd	R ₁	R ₂	R ₃	R ₄	PKa % inhibition		PKa IC ₅₀ (nM)	LE
					1000 nM	100 nM		
7a	H	H	H	H	29	0	n.d.	
7b	F	H	H	H	59	13	n.d.	
7c	Cl	H	H	H	67	12	n.d.	
7d	CH ₃	H	H	H	62	12	n.d.	
7e	OCH ₃	H	H	H	63	11	n.d.	
7f	H	Cl	H	H	74	20	n.d.	
7g	H	CH ₃	H	H	57	11	n.d.	
7h	H	OCH ₃	H	H	83	35	90	0.31
7i	H	H	Cl	H	60	13	n.d.	
7j	H	H	CH ₃	H	84	36	88	0.32
7k	H	H	OCH ₃	H	72	17	n.d.	
7l	F	H	H	F	88	47	62	0.32
7m	F	H	H	Cl	92	61	31	0.33
7n	F	H	H	CF ₃	97	83	7.8	0.32
7o	Cl	H	H	Cl	94	56	40	0.32
7p	CH ₃	H	H	CH ₃	89	53	68	0.31

^an.d., not determined.Table 5. Selected SARs from Substituted Phenyl P1 Groups^a

compd	R ₁	R ₂	R ₃	R ₄	PKa IC ₅₀ (nM)	Caco-2 P _{app} (×10 ⁻⁶ cm/s)	HLM CL _{int} (μL/min/mg protein)	kinetic sol 0.1 N HCl (mg/mL)	kinetic sol aq assay buffer (pH 7.4) (mg/mL)	cLogP ^b	LLE
13a	H	F	OCH ₃	F	3.0	3.2	36	n.d.	n.d.	2.4	6.1
13b	CH ₂ OCH ₃	F	OCH ₃	F	6.0	18	92	>0.12	>0.12	2.8	5.4
13c	CH ₂ N(CH ₃) ₂	F	OCH ₃	F	6.3	14	280	n.d.	n.d.	2.4	5.8
13d	CH ₂ OCH ₃	F	OCH ₃	H	17	25	45	>0.12	>0.12	2.6	5.2
13e	N(CH ₃) ₂	F	OCH ₃	H	73	23	120	>0.12	>0.12	2.7	4.4
13f	cyclopropyl	F	OCH ₃	H	23	24	170	>0.11	0.058–0.11	3.2	4.4
13g	CH ₂ OCH ₃	F	OH	H	440	n.d.	n.d.	>0.12	>0.12	2.2	4.2
13h	CH ₂ OCH ₃	F	CH ₂ CH ₃	H	140	n.d.	n.d.	0.029–0.059	>0.12	3.2	3.7
13i	CH ₂ OCH ₃	F	OCHF ₂	H	150	n.d.	n.d.	0.063–0.12	>0.12	2.6	4.2
13j	CH ₂ OCH ₃	F	OCH ₃	Cl	5.5	9.3	120	>0.12	>0.12	3.4	4.9
13k	CH ₂ OCH ₃	F	OCH ₃	CN	1.0	14	58	>0.12	>0.12	2.1	6.9
13l	CH ₂ OCH ₃	H	OCH ₃	F	35	n.d.	n.d.	>0.12	>0.12	2.4	5.1
13m	CH ₂ OCH ₃	CHF ₂	OCH ₃	F	6.8	11	100	>0.13	>0.13	3.1	5.1

^an.d., not determined. ^bcLogP values generated using ACD/Laboratories Percepta software.

core (15) significantly reduced the permeability and matched the trend previously observed. Other pyrazole core substituents were tolerated with 16 and 17 showing potencies and permeabilities similar to those of 14s and 14w. However, HLM CL_{int} values for 16 and 17 were slightly higher at 49 μL/min/mg of protein for both compounds. Of the two similar compounds, 16 was further profiled because of its clean off-target protease selectivity profile (Table S1).

Lead Profiling. Compounds 13b and 13k (phenyl P1 groups, methoxymethylpyrazole cores), 14s and 14w (pyridine P1 groups, methoxymethylpyrazole cores), and 16 (pyridine P1 group, trifluoromethylpyrazole core) all showed a favorable balance of PKa inhibition and encouraging in vitro ADME. Further selectivity profiling of these leads showed all had IC₅₀ values of >10 000 nM against a panel of closely related human serine proteases (FXIa, FXIIa, tissue kallikrein-1 [KLK1], thrombin, trypsin, and plasmin), with the exception of 14s,

Table 6. Selected SARs from Substituted Heterocyclic P1 Groups

compd	Het P1 group	PKa IC ₅₀ (nM)	compd	Het P1 group	PKa IC ₅₀ (nM)	compd	Het P1 group	PKa IC ₅₀ (nM)
14a		3700	14j		460	14s		4.1
14b		3000	14k		210	14t		3200
14c		460	14l		900	14u		37
14d		4200	14m		160	14v		93
14e		7900	14n		2200	14w		6.0
14f		2500	14o		250	14x		7.9
14g		2300	14p		900	14y		2400
14h		570	14q		140	14z		160
14i		220	14r		300			

which possessed weak thrombin inhibition (IC₅₀ of 7500 nM) but still had selectivity greater than 1800-fold relative to its IC₅₀ against PKa. Consequently, they were all progressed to animal pharmacokinetic (PK) studies (Table 8).

PK studies in Sprague-Dawley rats were conducted at a nominal 1 mg/kg iv and 10 mg/kg po dose (Table 8). Lead compounds showed similar iv PK profiles, with plasma clearances ranging from 7 to 16 mL/min/kg in the rat. **13b**, **14w**, and **16** all showed clearances at or below 1/3 of liver blood flow (LBF). The volume of distribution at the steady state (V_{ss}) for all examples was below 1 L; this feature is considered beneficial in restricting the inhibitors to the plasma

compartment where the biological target enzyme PKa is located. The rat oral bioavailability was more variable, ranging from 20% for **13k** to 97% for **16**. On the basis of the higher oral bioavailability observed in rats, compounds **13b**, **14w**, and **16** were selected for PK studies in beagle dogs. Studies were conducted at a nominal 1 mg/kg iv and 1 mg/kg po dose, and profiles similar to the rat pharmacokinetic studies were observed. Higher clearances were observed in the dog pharmacokinetic study, with **13b** showing a clearance of approximately 3/4 LBF and **16** showing a clearance approaching 1/2 LBF. The clearance of **14w** in the dog was similar to its clearance value in the rat at just over 1/3 LBF.

Table 7. Selected SARs from Neutral P1 Groups^a

compd	R ₁	R ₂	R ₃	X	PKa	IC ₅₀ (nM)	Caco-2 P _{app} (×10 ⁻⁶ cm/s)	HLM CL _{int} (μL/min/mg of protein)	solubility (mg/mL)		cLogP ^c	cLogD ^c pH 7.4/pH 6.5	LLE
									FaSSIF	FaSSGF			
13b	CH ₂ OCH ₃	F	OCH ₃	CF		6.0	18	92	0.009 ^{b,c}	0.009 ^{b,c}	2.8	2.8/2.8	5.4
13k	CH ₂ OCH ₃	F	OCH ₃	CCN		1.0	14	58	0.031 ^b	0.021 ^b	2.1	2.1/2.1	6.9
14s	CH ₂ OCH ₃	CH ₃	OCH ₃	N		4.1	25	25	0.11 ^b	0.97 ^b	2.0	1.9/1.8	6.4
14w	CH ₂ OCH ₃	F	OCH ₃	N		6.0	9.0	14	0.22 ^b , 0.11 ^{b,c}	>1.0 ^b , 11 ^{b,d}	1.8	1.8/1.8	6.4
14x	CH ₂ OCH ₃	F	OCH ₂ CH ₃	N		7.9	11	69	n.d.	n.d.	2.2	2.2/2.2	5.9
15	H	F	OCH ₃	N		5.1	3.1	2.0	n.d.	n.d.	1.5	1.5/1.5	6.8
16	CF ₃	F	OCH ₃	N		3.2	17	49	0.02 ^b	0.69 ^b	2.2	2.2/2.2	6.3
17	cyclopropyl	F	OCH ₃	N		4.4	9.5	49	n.d.	n.d.	2.0	2.0/2.0	6.4

^an.d., not determined. ^bTested at a theoretical concentration of 1 mg/mL. ^cSolubility was carried out on crystalline material. ^dTested at a theoretical concentration of 100 mg/mL. ^ecLogP and cLogD values generated using ACD/Laboratories Percepta software.

The leads **14w** and **16** containing pyridine P1 groups showed slightly higher volumes than **13b**, but all were still below 1 L. As a general trend, the bioavailabilities in the dog were lower compared with those in the rat. Compound **13b** showed a significant drop-off with a bioavailability of 16%, but the bioavailabilities of **14w** and **16** reached 34 and 32%, respectively. A whole plasma screening assay was developed to replicate in vivo kallikrein–kinin system activation during an HAE attack. PKa activity in whole plasma was measured in the presence of dextran sulfate (DXS) stimulation using a fluorogenic substrate. The assay was used to evaluate the potency of PKa inhibitors in preventing activation of the kallikrein–kinin system. Compounds **14w** and **16** stood out in the DXS-activated whole plasma assay as the most potent compounds (Table 9); **14w** performed especially well, with only a 1:9 potency ratio between the isolated enzyme IC₅₀ and whole plasma IC₅₀ values. We observed a correlation between the DXS-activated human whole plasma potencies and the free fraction of compound in the plasma. Compound **13b** has a human plasma protein binding (PPB) of 97% and is the least potent in the human whole plasma assay, **16** has a human PPB of 87% and improved human whole plasma potency, and **14w** has the lowest human PPB of the set at 77% and shows the best whole plasma IC₅₀ value at 54 nM. All three compounds demonstrated fast kinetics, another factor that has been shown to affect this assay.²³ hERG inhibition values were measured up to a maximum concentration of 33 μM for **13b**, **14w**, and **16** in the electrophysiology patch clamp assay (QPatch, Sophion Bioscience A/S, Ballerup, Denmark) using Chinese hamster ovary cells stably expressing the hERG channel. The IC₅₀ values obtained were >33 μM for all lead compounds (**13b**, **14w**, **16**), thus indicating that they were unlikely to cause a clinical change in ECG readings. The lead compounds were also tested against a panel of CYP450 enzymes up to 25 μM. **13b** was found to inhibit CYP450 enzyme 2C9 (IC₅₀ = 13 μM) and both subsites of CYP450 enzyme 3A4; these were tested using different substrates, midazolam (M) and testosterone (T) (3A4(M) IC₅₀ = 19 μM and 3A4(T) IC₅₀ = 11 μM). By contrast, both **14w** and **16** showed clean profiles up to the highest concentration tested. Ultimately, **14w** was nominated as a clinical candidate over **16** due to its clearance data (a lower human CL_{int} as well as clearances in percent LBF at or below 1/3 in both rat and dog PK studies), thermodynamic solubility (10-fold improvement in FaSSIF solubility), and its higher potency in the human PKa plasma activation assay.

Characterization of the Clinical Candidate **14w**.

Sebetralstat, **14w**, is a potent, competitive, and reversible inhibitor of human PKa (K_i = 3.0 nM) with fast kinetics (k_{on} > 10×10^6 M⁻¹ s⁻¹) and an acceptably high selectivity profile of >1500-fold against an extended panel of related human serine proteases (Table 10). It demonstrated acceptable solubility in FaSSIF (pH 6.5) and improved solubility in FaSSGF (pH 1.6) due to the ability of the pyridine nitrogen to be protonated at gastric pH (measured pK_a 3.6). The ability to dissolve in gastric fluids was considered a key advantage of **14w** that could facilitate fast dissolution and absorption in vivo. Sebetralstat, **14w**, demonstrated high selectivity against an off-target safety panel (Eurofins, St. Charles, MO, USA; 124 targets). At the highest level tested (33 μM), no significant inhibition of hERG channel was observed in the electrophysiology patch clamp assay, which reduced the potential for cardiovascular risk connected with QT prolongation. In CYP450 inhibition

Table 8. PK Parameters in Rat and Dog for Lead Compounds

compd	species	CL _p (mL/min/kg)	CL _b (mL/min/kg)	LBF ^a (%)	V _{ss} (L)	t _{1/2} (h)	F (%)
13b	rat	12.8	23.7	30	0.39	0.7	64
13k	rat	16.0	27.6	35	0.60	1.1	20
14s	rat	14.0	35.0	44	0.21	1.0	31
14w	rat	11.7	20.9	26	0.50	1.0	82
16	rat	7.1	11.1	14	0.31	1.1	97
13b	dog	11.5	24.5	74	0.36	0.5	16
14w	dog	8.7	10.9	33	0.65	1.0	34
16	dog	10.0	15.9	48	0.63	0.9	32

^aLiver blood flows used: rat, 80 mL/min/kg; dog, 33 mL/min/kg.²²

Table 9. PKa Plasma Activation Assay and Off-Target Safety Pharmacology

compd	human whole plasma (DXS activation 6.25 μg/mL) PKa IC ₅₀ (nM)	potency ratio isolated IC ₅₀ :plasma IC ₅₀	hERG ^a (μM)	CYP450 inhibition (μM)							
				1A2	2B6	2C8	2C9	2C19	2D6	3A4(M)	3A4(T)
13b	500	1:84	>33	>25	>25	14	13	>25	>25	19	11
14w	54	1:9	>33	>25	>25	>25	>25	>25	>25	>25	>25
16	76	1:24	>33	>25	n.d.	n.d.	>25	>25	>25	>25	>25

^ahERG measured using a whole cell (Chinese hamster ovary) patch clamp technique.

Table 10. Sebetralstat Protease Selectivity

enzyme	IC ₅₀ ^a (nM)	fold to PKa IC ₅₀
plasma kallikrein	6.0	—
tissue kallikrein (KLK1)	>40000	>6667
factor XIIa	>40000	>6667
factor XIa	>40000	>6667
factor Xa	>10000	>1667
factor VIIa	>10000	>1667
plasmin	>40000	>6667
thrombin	>40000	>6667
trypsin	>40000	>6667
β-secretase 1	>10000	>1667
cathepsin D	>10000	>1667
cathepsin G	>10000	>1667
renin	>10000	>1667
tissue plasminogen activator	>10000	>1667
tryptase	>10000	>1667

^aIC₅₀ values for sebetralstat inhibition of PKa and related proteases in isolated enzyme kinetic fluorogenic substrate assays.

(human liver microsomes), **14w** showed IC₅₀ data of >25 μM across the seven major isoforms, which predicted a minimal risk of associated drug–drug interactions. Several different CYP450 isoforms were found to contribute significantly to the clearance of **14w**, resulting in a lower risk of it being a victim of a CYP-mediated drug–drug interaction. Additionally, **14w** was screened in a non-GLP bacterial mutagenicity Ames test and showed no risk of genotoxicity.

We believe the excellent selectivity profile of **14w** is due to the induced fit around the benzylpyridone P4 group arising from the Trp215 movement on binding **14w**, together with the fine-tuning of the substituents and substitution pattern around the pyridine P1 group. The crystal structure of **14w** complexed with PKa was solved by single crystal X-ray crystallography with a resolution of 2.06 Å using a soaking protocol previously reported in the literature.²⁴ The binding mode of **14w** within the active site was consistent with the previously reported crystal structure of benzylpyrazole PKa inhibitors²⁵ showing the characteristic U-shaped conformation about the central

pyrazole core. This conformation is enabled by the movement of Trp215 (“Trp flip”) that forms an induced hydrophobic pocket wherein the ligand makes a network of π -stacking interactions with the protein in addition to the hydrogen bond with Gly99 (Figure 4).

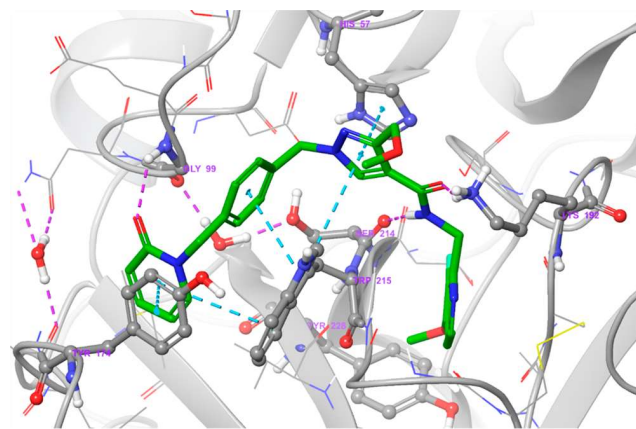


Figure 4. Crystal structure of **14w** complex with PKa (PDB code 8A3Q). The characteristic U-shaped conformation is stabilized by the movement of Trp215 (“Trp flip”) that enables a network of π -stacking interactions with the ligand: Tyr174/terminal pyridone (face-to-face); Trp215/phenyl linker (face-to-face) and pyrazole core (edge-to-face); His57/pyrazole core (face-to-face). A total of three hydrogen bonds are observed: Gly99 backbone N–H/pyridone carbonyl, Ser214 backbone carbonyl/amide N–H, and Lys192 side chain N–H/amide carbonyl. The pyridine P1 group occupies the S1 subpocket without forming specific polar interactions with any of the amino acids including Asp189. Image created using Maestro (Schrödinger, New York, NY, USA).

An analysis of the occupation of **14w** in the S1 pocket showed unique and unexpected features. As expected, with the lack of a strongly basic P1 group, the previously described salt bridge with Asp189 was absent. However, no other specific polar interactions were observed with any of the amino acids lining the S1 pocket; thus, the reason for the exquisite affinity

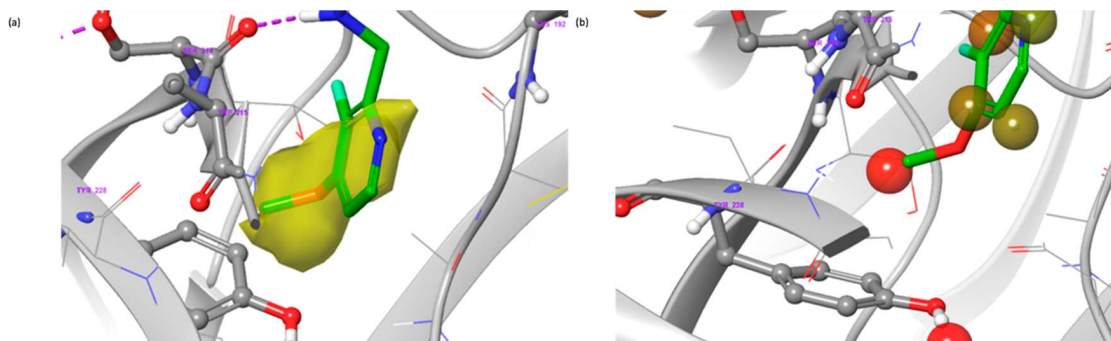


Figure 5. (a) P1 group in **14w** in relation to the S1 hydrophobic region (yellow volume, calculated with SiteMap). (b) Analysis of predicted water molecules in the unbound form of the S1 pocket (calculated with WaterMap and the relative energy level in a color scale of green (favorable free energy) to red (unfavorable free energy)). A high energy water in the proximity of Tyr228 is displaced by the methoxy group upon binding in the S1 pocket.

of the disubstituted pyridine P1 group was initially puzzling. Further analyses of the hydrophobicity and hydration of the S1 pocket were therefore performed (Figure 5). Profiling the pocket with SiteMap (Schrödinger, New York, NY, USA) showed that the 4-methoxy substituent occupies the hydrophobic volume present at the bottom of the pocket. Accordingly, we concluded that part of the gain in affinity was due to beneficial hydrophobic interactions. Nevertheless, this observation did not explain the steep SAR observed in the pyridine *meta*-position where methoxy was preferred to other more lipophilic substituents such as chlorine and methyl. To resolve this conundrum, a molecular dynamics simulation of the water molecules in the unbound protein (*apo* form) was performed, and their thermodynamic properties were calculated with WaterMap (Schrödinger, New York, NY, USA). It was observed that a water molecule, predicted to lie above the face of Tyr228, was calculated to have an unfavorable free energy due to its positioning in a lipophilic local environment. This water molecule was not detected in the crystal structure. Consequently, we hypothesized that displacement of the “unhappy” water molecule by the methoxy group favorably contributes to the binding affinity. Overall, it is believed that the combination of lipophilic interactions and the displacement of the high energy water molecule make the 3-fluoro-4-methoxypyridine P1 group exquisitely tailored to the S1 pocket, thus removing the need for the ionic interaction with Asp189. Analysis of the crystal structure also allowed the rationalization of SAR in other parts of the scaffold such as the central pyrazole core. The methoxymethylene side chain was heavily solvent exposed, which explained the tolerance of diverse substituents observed in this region.

On the basis of the promising data described in this paper, the pharmacological suppression of the kallikrein–kinin system in whole plasma,²¹ and results from investigational new drug-enabling studies, **14w** was advanced into human clinical trials for the on-demand treatment of HAE attacks. The phase 1 clinical trials in healthy volunteers demonstrated that the human pharmacokinetic profile matched the desired on-demand treatment profile with rapid absorption of sebetralstat and near-complete inhibition of PKa enzyme activity determined using PKa assay in whole plasma (Figure 6).²⁶

Chemistry. We describe the preparation of **14w** here in detail. Syntheses of the other derivatives (**3–6**, **7a–7p**, **8**, **9a–9n**, **10–12**, **13a–13m**, **14a–14v**, **14x–14z**, **15–17**) are described in the Supporting Information or in filed patents where referenced. The synthesis of **14w** is described in Scheme

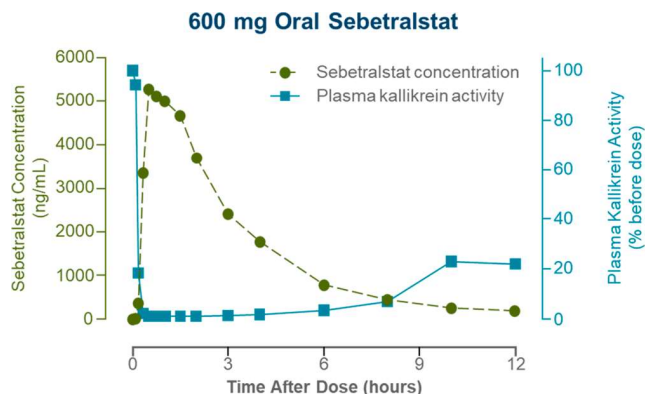
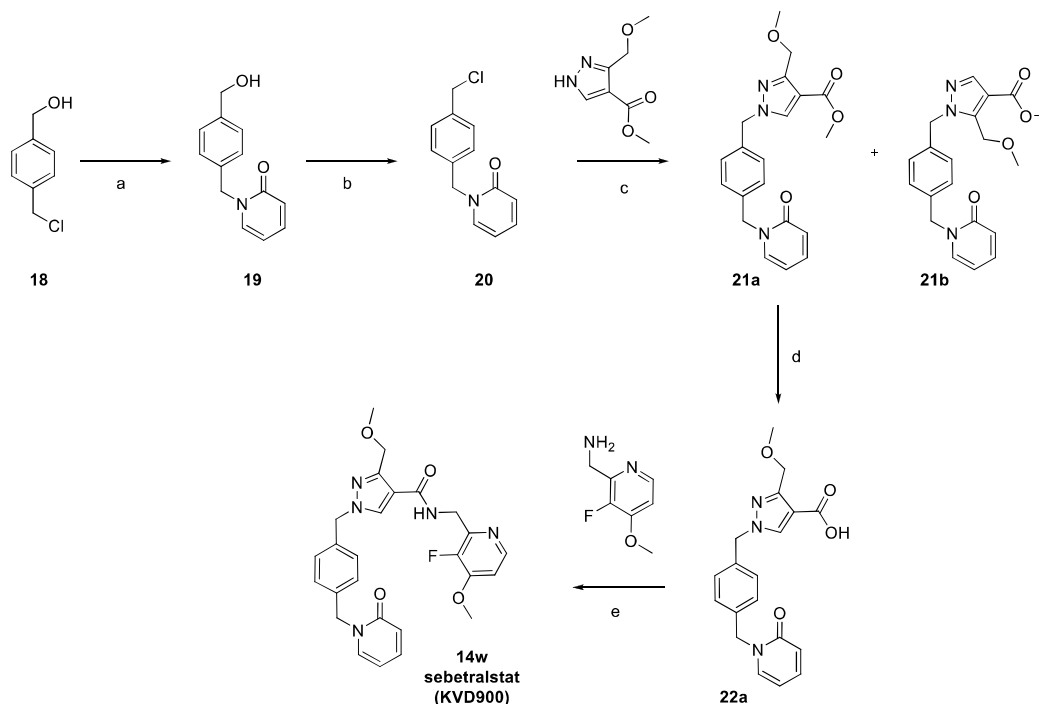


Figure 6. Green line shows the rapid oral absorption of sebetralstat in healthy volunteers. Blue line shows the effect of sebetralstat on percentage PKa activity. From ref 26. CC BY NC ND.

1. Reaction of 4-(chloromethyl)benzyl alcohol (CAS No. 16473-35-1), **18**, with 2-hydroxypyridine in the presence of potassium carbonate occurred regioselectively to give the *N*-benzylpyridone alcohol **19**. Regioisomeric assignment was determined by NMR²⁷ using through-bond information (¹H–¹³C HSQC and ¹H–¹³C HMQC) and through-space distance information (NOESY) (Figure 7).

Conversion of the hydroxyl function in the *N*-benzylpyridone alcohol **19** to the corresponding chloride **20** proceeded via the methanesulfonate intermediate. *N*-Alkylation of 3-methoxymethyl-1*H*-pyrazol-4-carboxylic acid methyl ester (synthesized according to the method described in WO 2012/009009,²⁸ now commercially available CAS No. 318496-66-1) gave a mixture of regioisomers in favor of the desired isomer **21a** that was isolated in 47% yield by column chromatography. Regioisomeric assignments were determined with NMR experiments (NOESY, ¹H–¹³C HSQC, and ¹H–¹³C HMQC) (Figure 8). The assigned regiochemistry was confirmed once the X-ray crystal structure for **14w** was obtained. Subsequent hydrolysis of **21a** gave the carboxylic acid **22a** that was then coupled with C-(3-fluoro-4-methoxypyridin-2-yl)-methylamine (synthesized according to the method described in US 10,781,181,²⁹ now commercially available CAS No. 1256812-75-5) via a HATU-mediated amidation to afford **14w** in 64% yield as a white solid.

Scheme 1. Synthesis of Sebetralstat^a

^aReagents and conditions: (a) 2-Hydroxypyridine (1.2 equiv), K₂CO₃ (3.0 equiv), acetone, 50 °C, 18 h, 78%; (b) methanesulfonyl chloride (1.3 equiv), Et₃N, (1.4 equiv), dichloromethane, rt, 18h, 93%; (c) methyl 3-(methoxymethyl)-1H-pyrazole-4-carboxylate (0.83 equiv), K₂CO₃ (2.0 equiv), DMF, 60 °C, 18 h, 54%; (d) NaOH (3.0 equiv), THF-MeOH-H₂O, rt, 18 h, 34%; (e) **22a** (1.0 equiv), C-(3-fluoro-4-methoxy-pyridin-2-yl)-methylamine (1.0 equiv), HATU (1.1 equiv), Et₃N (6.0 equiv), dichloromethane, rt, 4 h, 64%.

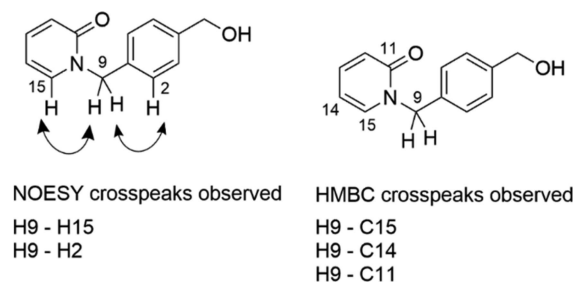


Figure 7. NMR assignments for **19**. NOESY and HMBC crosspeaks shown. NMR spectral analyses are included in the [Supporting Information](#).

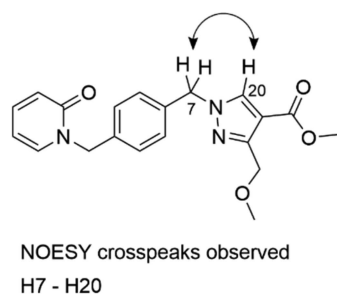


Figure 8. NMR assignments for **21a**. NOESY crosspeaks shown. NMR spectral analyses are included in the [Supporting Information](#).

CONCLUSIONS

The design of sebetralstat (KVD900), an orally bioavailable, selective, and neutral PKa inhibitor, has been described. The SAR information collected from the early PKa inhibitor series

enabled the discovery of the highly potent scaffold exemplified in compounds **4** and **6** with benzylpyridone P4 and pyrazole amide core. This led us to investigate new binding modalities within the P1 pocket that did not rely on the ionic interaction with Asp189. Compound **6** with benzylpyridone P4 and pyrazole amide core was considered an ideal starting point for the design of a library of substituted phenyl P1 groups. The SAR obtained from the library facilitated the identification of the preferred *o-o*-difluoro-*m*-methoxy substitution pattern that produced the 3 nM inhibitor **13a** devoid of a basic P1 group. Lead optimization of **13a** introduced two important innovations: (1) the substitution of the pyrazole core, which improved permeability; (2) the pyridine P1 group exemplified in compound **14w**, which reduced the lipophilicity and increased solubility. X-ray analysis of key molecules during the project progression demonstrated several interesting features. First, all our observed X-ray structures induced a rotamer flip of Trp215 compared with the benzamidine-bound structure (PDB code 2ANW). This rotamer flip opens a deep S4 binding pocket resulting in characteristic U-shaped binding conformations to PKa, unusual in this class of serine proteases. Second, exploration of the S1 pocket and discovery of neutral P1 groups has identified significant alternative opportunities in P1 binding, particularly highlighting the importance of hydrophobic interactions. Furthermore, the novel 3-fluoro-4-methoxypyridine P1 group derives favorable binding energy via displacement of a water molecule close to Tyr228. These innovations, which resulted in profoundly different molecular properties, led to the discovery of sebetralstat. This PKa inhibitor showed no issues in off-target pharmacology and possessed high selectivity against related human serine proteases. These features, together with the rapid and high

plasma exposure and near-complete inhibition of PKa in preclinical studies, supported its progression into toxicology assessments and ultimately clinical evaluation. Pharmacokinetic and pharmacodynamic profiles demonstrating rapid and near-complete PKa inhibition were observed in healthy patients from the phase 1 study. Sebetralstat was shown to provide fast symptom relief in a phase 2 study in patients with HAE, and this investigational on-demand treatment has advanced to a phase 3 clinical study.^{23,30}

EXPERIMENTAL SECTION

General Chemistry Methods. All reactions were carried out with commercial grade reagents and solvents and were used without further purification. NMR chemical shifts (δ) are reported in parts per million and were recorded on a Bruker (400 MHz) spectrometer (Billerica, MA, USA) with reference to deuterium solvent or tetramethylsilane and run at ambient temperature. Flash chromatography was carried using silica gel for chromatography, 0.035–0.070 mm (220–440 mesh) (e.g., Merck silica gel 60, Rahway, NJ, USA) or prepacked silica cartridges and eluted with gradients of the specified solvents. Preparative reverse phase HPLC was carried out on C18 HPLC columns using acetonitrile/water gradients containing 0.1% trifluoroacetic acid. Purities of all final compounds were determined to be $\geq 95\%$ by analytical HPLC. HPLC data were collected with the use of an Agilent 1100 HPLC system with UV detection (Santa Clara, CA, USA) and a Thermo Hypersil Gold C18 4.5 \times 150 mm 5.0 mm column (Thermo Fisher Scientific, Waltham, MA, USA). The conditions were as follows: mobile phase A, –0.1% trifluoroacetic acid in acetonitrile; mobile phase B, –0.1% trifluoroacetic acid in water; flow rate 1.5 mL/min; gradient 2–98% B over 30 min. LC–MS data were collected with the use of a Waters Acquity H-Class LC system equipped with a Waters Acquity QDa mass spectrometer with ESI (Milford, MA, USA) and a Waters Acquity UPLC BEH C18 2.1 \times 50 mm 1.7 mm column. The conditions were as follows: mobile phase, –0.1% formic acid in acetonitrile; mobile phase B, –0.1% formic acid in water; flow rate 1.0 mL/min; gradient 2–98% B over 3 min.

Synthesis of Sebetralstat. 1-(4-Hydroxymethyl-benzyl)-1H-pyridin-2-one (**19**). 4-(Chloromethyl)benzyl alcohol **18** (5.0 g, 31.9 mmol) was added to a solution of potassium carbonate (13.2 g, 96 mmol) and 2-hydroxypyridine (3.6 g, 38.3 mmol) in acetone (250 mL). The reaction mixture was heated at 50 °C for 18 h and then concentrated in vacuo. The residue was partitioned between dichloromethane (300 mL) and water (300 mL). The organic layer was separated, and the aqueous layer was extracted with dichloromethane (2 \times 300 mL). The combined organic layers were washed with brine (300 mL), dried over magnesium sulfate, filtered, and concentrated in vacuo. The residue was purified by flash chromatography on silica (0–10% methanol in dichloromethane) to afford **19** (5.4 g, 25.1 mmol, 78% yield) as a white solid. MS (ESI) m/z 216.0 ($M + H$)⁺. ¹H NMR (400 MHz, DMSO- d_6) δ 7.76 (dd, J = 6.8, 2.1 Hz, 1H), 7.41 (ddd, J = 9.0, 6.6, 2.1 Hz, 1H), 7.34–7.21 (m, 4H), 6.41 (dd, J = 9.1, 1.3 Hz, 1H), 6.22 (td, J = 6.7, 1.4 Hz, 1H), 5.15 (t, J = 5.7 Hz, 1H), 5.07 (s, 2H), 4.46 (d, J = 5.7 Hz, 2H). ¹³C NMR (100 MHz, DMSO- d_6) δ 161.4, 141.9, 140.0, 139.0, 135.7, 127.5, 126.6, 119.8, 105.4, 62.6, 50.8.

1-(4-Chloromethyl-benzyl)-1H-pyridin-2-one (**20**). A reaction flask containing 1-(4-hydroxymethyl-benzyl)-1H-pyridin-2-one (**19**) (8.45 g, 39.3 mmol), dry dichloromethane (80 mL), and triethylamine (7.66 mL, 55.0 mmol) was cooled in an ice–water bath. Methanesulfonyl chloride (3.95 mL, 51.0 mmol) was added to the reaction at 0 °C, and ice–water bath cooling continued. After 15 min, the ice–water bath was removed and stirring continued at room temperature overnight. The reaction mixture was partitioned between dichloromethane (100 mL) and saturated aqueous ammonium chloride solution (100 mL). The aqueous layer was extracted with further dichloromethane (2 \times 50 mL), and the combined organic layers were washed with brine (50 mL), dried over sodium sulfate, filtered, and concentrated to afford **20** (8.65 g, 36.6 mmol, 93% yield)

as a pale yellow solid. MS (ESI) m/z 234.1 ($M + H$)⁺. ¹H NMR (400 MHz, DMSO- d_6) δ 7.79 (ddd, J = 6.8, 2.1, 0.7 Hz, 1H), 7.49–7.39 (m, 1H), 7.40 (d, J = 7.8 Hz, 2H), 7.28 (d, J = 8.4 Hz, 2H), 6.42 (ddd, J = 9.2, 1.3, 0.7 Hz, 1H), 6.24 (td, J = 6.7, 1.4 Hz, 1H), 5.09 (s, 2H), 4.73 (s, 2H). ¹³C NMR (101 MHz, DMSO- d_6) δ 161.4, 140.1, 139.1, 137.6, 136.9, 129.0, 127.9, 119.9, 105.5, 50.8, 45.8.

Methyl 3-(Methoxymethyl)-1-(4-((2-oxopyridin-1(2H)-yl)methyl)benzyl)-1H-pyrazole-4-carboxylate (**21a**) and Methyl 5-(Methoxymethyl)-1-(4-((2-oxopyridin-1(2H)-yl)methyl)benzyl)-1H-pyrazole-4-carboxylate (**21b**). Methyl 3-(methoxymethyl)-1H-pyrazole-4-carboxylate (2.11 g, 11.77 mmol; CAS No. 318496-66-1) was added to a solution of potassium carbonate (3.25 g, 23.54 mmol) and 1-(4-chloromethyl-benzyl)-1H-pyridin-2-one **20** (3.30 g, 14.12 mmol) in *N,N*-dimethylformamide (5 mL) and heated at 70 °C for 3 h. The reaction mixture was diluted with ethyl acetate (50 mL) and washed with brine (2 \times 100 mL), and the organic layer was dried over magnesium sulfate, filtered, and concentrated in vacuo. The crude product was purified by flash chromatography (120 g column, 0–100% (10% ethanol in ethyl acetate) in isohexanes to afford two regioisomers: **21a** (2.03 g, 5.47 mmol, 47% yield) as an off-white solid and **21b** (350 mg, 0.92 mmol, 8% yield). **21a** MS (ESI) m/z 368.1 ($M + H$)⁺. ¹H NMR (400 MHz, DMSO- d_6) δ 8.42 (s, 1H), 7.76 (dd, J = 6.8, 2.2 Hz, 1H), 7.41 (ddd, J = 8.9, 6.5, 2.1 Hz, 1H), 7.25 (d, J = 1.2 Hz, 4H), 6.40 (dt, J = 9.1, 1.0 Hz, 1H), 6.22 (td, J = 6.7, 1.4 Hz, 1H), 5.30 (s, 2H), 5.07 (s, 2H), 4.49 (s, 2H), 3.72 (s, 3H), 3.23 (s, 3H). ¹³C NMR (101 MHz, DMSO- d_6) δ 163.2, 161.8, 150.5, 140.6, 139.6, 137.6, 136.3, 135.6, 128.5, 128.4, 120.3, 111.8, 106.0, 66.0, 58.0, 55.1, 51.5, 51.2. **21b** MS (ESI) m/z 368.1 ($M + H$)⁺. ¹H NMR (400 MHz, DMSO- d_6) δ 7.88 (s, 1H), 7.76 (dd, J = 6.8, 2.1 Hz, 1H), 7.41 (ddd, J = 8.9, 6.6, 2.1 Hz, 1H), 7.28–7.21 (m, 2H), 7.17 (d, J = 8.2 Hz, 2H), 6.43–6.36 (m, 1H), 6.22 (td, J = 6.7, 1.4 Hz, 1H), 5.35 (s, 2H), 5.06 (s, 2H), 4.78 (s, 2H), 3.75 (s, 3H), 3.25 (s, 3H). ¹³C NMR (101 MHz, DMSO- d_6) δ 163.4, 161.8, 142.4, 140.9, 140.5, 139.6, 137.4, 136.2, 128.3, 120.3, 112.8, 106.0, 61.7, 58.2, 53.0, 51.7, 51.2.

3-(Methoxymethyl)-1-(4-((2-oxopyridin-1(2H)-yl)methyl)benzyl)-1H-pyrazole-4-carboxylic acid (**22a**). To methyl 3-(methoxymethyl)-1-(4-((2-oxopyridin-1(2H)-yl)methyl)benzyl)-1H-pyrazole-4-carboxylate **21a** (3.77 g, 10.26 mmol) in tetrahydrofuran (5 mL) and methanol (5 mL) was added 2 M aqueous sodium hydroxide solution (15.39 mL, 30.80 mmol), and the reaction mixture was stirred at room temperature overnight. The reaction was acidified with 1 M aqueous HCl solution (50 mL) and extracted with ethyl acetate (50 mL). The organic layer was washed with brine (50 mL), dried over magnesium sulfate, filtered, and concentrated in vacuo to afford **22a** (1.22 g, 3.45 mmol, 34% yield) as a white solid. MS (ESI) m/z 354.2 ($M + H$)⁺. ¹H NMR (400 MHz, DMSO- d_6) δ 12.32 (s, 1H), 8.32 (s, 1H), 7.76 (ddd, J = 6.8, 2.1, 0.7 Hz, 1H), 7.41 (ddd, J = 8.9, 6.6, 2.1 Hz, 1H), 7.30–7.20 (m, 4H), 6.40 (ddd, J = 9.1, 1.4, 0.7 Hz, 1H), 6.22 (td, J = 6.7, 1.4 Hz, 1H), 5.29 (s, 2H), 5.07 (s, 2H), 4.50 (s, 2H), 3.22 (s, 3H). ¹³C NMR (101 MHz, DMSO- d_6) δ 164.3, 161.8, 150.5, 140.6, 139.6, 137.6, 136.4, 135.6, 128.5, 128.4, 120.3, 113.0, 106.0, 66.0, 58.0, 55.1, 51.2.

3-Methoxymethyl-1-[4-(2-oxo-2H-pyridin-1-ylmethyl)-benzyl]-1H-pyrazole-4-carboxylic Acid (3-Fluoro-4-methoxy-pyridin-2-ylmethyl)-amide (**14w**). 3-(Methoxymethyl)-1-(4-((2-oxopyridin-1(2H)-yl)methyl)benzyl)-1H-pyrazole-4-carboxylic acid **22a** (75 mg, 0.212 mmol), C-(3-fluoro-4-methoxy-pyridin-2-yl)-methanamine (49 mg, 0.212 mmol; CAS No. 1256812-75-5), and HATU (89 mg, 0.233 mmol) were suspended in anhydrous dichloromethane (3 mL) to which triethylamine (177 μ L, 1.270 mmol) was added, sonicated, and then left to stir at room temperature for 4 h. The solvent was removed under reduced pressure, and the resulting residue was quenched with saturated aqueous ammonium chloride solution (5 mL). An off-white solid resulted, which was sonicated, filtered under reduced pressure, washed with water, and dried in a vacuum oven at 40 °C overnight. The residue was purified by chromatography eluting with 1% NH₃ in MeOH/dichloromethane to afford **14w** as a white solid (67 mg, 64% yield). MS (ESI) m/z 492.0 ($M + H$)⁺. ¹H NMR (400 MHz, DMSO- d_6) δ : 8.42 (t, J = 5.4 Hz, 1H), 8.29–8.21 (m, 2H), 7.75 (ddd, J = 0.7,

2.1, 6.8 Hz, 1H), 7.41 (ddd, $J = 2.1, 6.6, 8.9$ Hz, 1H), 7.28–7.17 (m, 5H), 6.39 (ddd, $J = 0.7, 1.4, 9.2$ Hz, 1H), 6.22 (td, $J = 1.4, 6.7$ Hz, 1H), 5.28 (s, 2H), 5.07 (s, 2H), 4.57–4.46 (m, 4H), 3.92 (s, 3H), 3.25 (s, 3H). ^{13}C NMR (101 MHz, DMSO- d_6) δ 161.9, 161.3, 153.0 ($J_{\text{C-F}} = 8.7$ Hz), 147.5, 146.8 ($J_{\text{C-F}} = 253.5$ Hz), 146.0 ($J_{\text{C-F}} = 7.2$ Hz), 145.2 ($J_{\text{C-F}} = 11.6$ Hz), 140.1, 139.1, 137.1, 136.0, 133.2, 128.1, 127.9, 119.9, 116.3, 108.7, 105.5, 66.3, 57.5, 56.4, 54.6, 50.7, 38.3.

General Biological Methods. *Determination of Percentage Inhibition and IC_{50} for PKa and Related Proteases (Isolated Enzyme).* PKa inhibitory activity in vitro was determined with the use of standard published methods.³¹ Following preincubation for 5 min, the enzymatic activity was analyzed with kinetic assays of fluorogenic substrate cleavage using a fluorometer (Spark 20M, Tecan, Männedorf, Switzerland). Human PKa (Calbiochem, MilliporeSigma, Burlington, MA, USA) activity was measured by using H-D-Pro-Phe-Arg-AFC (Peptide Protein Research, Southampton, Hampshire, U.K.). To estimate the IC_{50} , a four-parameter logistic dose–response curve was fitted to the normalized rate of fluorescence increase. The effects of **14w** on the catalytic activity of a panel of serine proteases (Table 10) were analyzed by using fluorogenic substrate cleavage assays specific for each protease using standard published methods.^{32,33} The compound was preincubated with each enzyme for 5 min prior to substrate addition. To estimate the IC_{50} , a four-parameter logistic dose–response curve was fitted to the normalized rate of fluorescence increase. The active proteases typically purified from human plasma and corresponding substrates are commercially available.

Determination of PKa Activity in Whole Plasma. PKa enzyme activity was measured in human pooled plasma (control plasma, Affinity Biologicals, Ancaster, Ontario, Canada) by using H-D-Pro-Phe-Arg-AFC. The kallikrein–kinin system in plasma was stimulated by the addition of DXS 500 kDa (Sigma-Aldrich, St. Louis, MO, USA). PKa activity in the plasma was estimated based on the maximum rate of fluorescence increase. To determine the PKa plasma IC_{50} , compounds (at eight concentrations) were preincubated for 5 min in control plasma prior to DXS stimulation. Plasma samples were stimulated with 6.25 $\mu\text{g}/\text{mL}$ DXS, and PKa enzyme activity was measured as described above.

Caco-2 Permeability Assay. In vitro permeability was determined by using the Caco-2 model for oral absorption. The methodology was adapted from standard published methods.³⁴ The Caco-2 cells (ATCC, Global Biological Resource Center, Manassas, VA, USA) were seeded at a density of 2×10^5 cells/well on 24-well fibrillar collagen PET insert plates, 1 μm pore size (Corning Life Sciences, Tewksbury, MA, USA), and maintained for 3 days in Corning Intestinal Epithelium Differentiation Medium in a humidified incubator at 5% CO_2 . For the assay, test compounds were prepared in DMSO and diluted 100-fold in Tyrode's buffer pH 7.4 (Sigma-Aldrich) and added to the apical side of the insets with Tyrode's buffer added to the basolateral compartment. Assay plates were incubated for 1 h at 37 $^\circ\text{C}$ on a shaking platform (120 rpm). Apical to basolateral transport was determined by measuring the test article in both compartments by LC–MS/MS following incubation. The integrity of the Caco-2 monolayers was confirmed by two methods: (1) comparison of pre- and postexperiment transepithelial electrical resistances and (2) assessment of Lucifer Yellow flux. P_{app} was calculated as $(V_{\text{B}}/(\text{AUC}_{\text{A}} + \text{AUC}_{\text{B}}))((1/S)(\text{AUC}_{\text{B}}/t))$, where V_{B} is the volume of Tyrode's buffer in the basolateral compartment, AUC_{A} is the total peak area of the test drug in the apical compartment postincubation, AUC_{B} is the total peak area of the test drug in the basolateral compartment postincubation, S is the surface area of the monolayer, and t is the incubation time.

In Vitro Clearance Determinations with Human Liver Microsomes. The CL_{int} in human liver microsomes was determined by using standard published methods.³⁵ For the assay, test compounds were prepared in 50:50 DMSO:acetonitrile and mixed with human liver microsomes (0.5 mg/mL; BD Gentest, Woburn, MA, USA) in 0.1 M phosphate buffer at a final substrate concentration of 5 μM . Reactions were initiated by the addition of NADPH-regenerating system with the assay plate shaking (150 rpm) at 37 $^\circ\text{C}$ for the

duration of the assay. Samples were taken at 0, 6, 12, 18, 24, and 60 min, and test compound concentrations were determined by LC–MS/MS against a calibration curve. The intrinsic clearance was calculated with methodology described in the literature.^{36,37}

The absorbance of the plate was read in the SpectraMax Plus plate reader (Molecular Devices, San Jose, CA, USA) at 25 $^\circ\text{C}$ at 650 nm before the addition of DMSO stock compound solutions. The stock compounds (10 mM in 100% DMSO) were then added at 0.1 μL quantities to 83 μL of (a) 0.1 N HCl (Sigma-Aldrich) or (b) Tyrode's buffer pH 7.6 (Sigma-Aldrich) plus 1% DMSO (Sigma-Aldrich) and 1% bovine serum albumin. Thus, 0.1 μL gave 12 μM , 0.2 μL gave 24 μM , etc. After the last additions, the plate was mixed for 30 s on a Variomag Teleshake (Thermo Fisher Scientific) at a quarter speed and then transferred to the SpectraMax Plus plate reader, where the absorbance was measured at 650 nm. Plate wells containing absorbances above 0.005 were checked under a microscope for foreign contamination prior to reporting results.

Thermodynamic Solubility. FaSSiF/FaSSiF/FaSSGF powder (Biorelevant, London, U.K.) was made up to the relevant buffer according to the manufacturer's instructions.³⁸

FaSSiF Solubility. The solubilities of test compounds in FaSSiF were determined at pH 6.5 after 4 h of equilibration at room temperature.

FaSSGF Solubility. The solubilities of test compounds in FaSSGF were determined at pH 1.6 after 4 h of equilibration at room temperature. Volumes of FaSSiF/FaSSiF/FaSSGF powder were added to test compounds to give nominal concentrations of either 1 or 100 mg/mL (as free base) in (preheated to 37 $^\circ\text{C}$) media. The samples were vortexed before being placed in a Titramax 1000 shaker (Heidolph Instruments, Schwabach, Germany) for 4 h at 37 $^\circ\text{C}$ and approximately 500 rpm. On completion, the samples were transferred to Eppendorf tubes and centrifuged at 15000g (relative centrifugal force) for 10 min at 37 $^\circ\text{C}$. Aliquots were taken and diluted, and the assay was run against calibration standards.³⁹

Pharmacokinetics. Rats. Pharmacokinetic studies were performed to assess the pharmacokinetics following a single iv or po dose in male Sprague-Dawley rats sourced from Charles River Laboratories (Harlow, Essex, U.K.). Two rats were given a single dose: 1 mg/kg iv as 1 mL/kg of a nominal 1 mg/mL formulation of test compound in vehicle or 10 mg/kg po as 5 mL/kg of a 2 mg/mL formulation of test compound in vehicle.

Dogs. Pharmacokinetic studies were performed to assess the pharmacokinetics following a single iv or oral po dose in male beagle dogs sourced from either Harlan UK (Blackthorn, Oxfordshire, U.K.) or Pharmaron Biologics (Cardiff, Wales, U.K.). Two dogs were given a single dose: 1 mg/kg IV as 1 mL/kg of a nominal 1 mg/mL formulation of test compound in vehicle or 1 mg/kg po as 5 mL/kg of a 0.2 mg/mL formulation of test compound in vehicle.

Following dosing, blood samples were collected over a period of 24 h. Sample times were 2, 5, 15, and 30 min and then 1, 2, 4, 6, and 12 h following iv administration and 5, 15, and 30 min and then 1, 2, 4, 6, 8, 12, and 24 h following oral administration. Following collection, blood samples were centrifuged, and the plasma fraction was analyzed for the concentration of the test compound by LC–MS. Pharmacokinetic parameters were determined with noncompartmental analysis.⁴⁰

hERG Inhibition. The QT prolongation potential of sebetralstat was evaluated by in vitro inhibition of the human hERG K^+ channel performed with whole-cell patch clamp electrophysiology.

CYP450 Inhibition Assay. Isoform-specific assay conditions were employed. Test compound (0.1, 0.25, 1, 2.5, 10, 25 μM) was incubated with pooled human liver microsomes (0.25 mg/mL; Corning Life Sciences), an appropriate isoform-specific probe substrate, and NADPH (1 mM) at 37 $^\circ\text{C}$ for an isoform-specific incubation time. The reactions were terminated by the addition of an aliquot of the incubation into methanol. The samples were centrifuged at 2500 rpm for 30 min at 4 $^\circ\text{C}$, and aliquots of the supernatant were diluted for LC–MS/MS analysis. The formation of isoform-specific metabolites acetaminophen (CYP 1A2), hydroxybupropion (CYP 2B6), 6 α -hydroxypaclitaxel (CYP 2C8), 4 hydrox-

ydiclofenac (CYP 2C9), 4-hydroxymephenytoin (CYP 2C19), dextrophan (CYP 2D6), 1-hydroxymidazolam, and 6 β -hydroxytestosterone (CYP 3A4) were monitored. A decrease in the amount of metabolite formed compared with vehicle control was used to calculate an IC₅₀ value for each experimental condition.

Ethical Statement. All scientific procedures on living animals conducted in the United Kingdom are subject to legislation under the Animals (Scientific Procedures) Act 1986. The Act is administered by the U.K. Home Office and provides for establishment designation, issue of project license for specified programs of work, and issue of personal licenses for individuals conducting procedures. All animal studies conducted were ethically reviewed and carried out in accordance with this Act, U.K. Home Office guidance on the implementation of the Act, and the Pharmaron UK Ltd. codes of practice for the care and housing of laboratory animals.

■ ASSOCIATED CONTENT

SI Supporting Information

The Supporting Information is available free of charge at <https://pubs.acs.org/doi/10.1021/acs.jmedchem.2c00921>.

Off-target protease selectivity table; synthesis of compounds 3–6, 7a–7p, 8, 9a–9n, 10–12, 13a–13m, 14a–14v, 14x–14z, and 15–17; NMR and HPLC spectra for intermediates 19, 20, 21a, 21b, and 22a and sebetralstat (14w); crystallographic information for 14w (PDF)

Molecular formula strings and reported data (CSV)

Accession Codes

Atomic coordinates and structure factors for the crystal structure of PKa with 14w are deposited in the Protein Data Bank (www.rcsb.org) with accession code 8A3Q.

■ AUTHOR INFORMATION

Corresponding Author

Rebecca L. Davie — KalVista Pharmaceuticals Limited, Salisbury SP4 0BF, U.K.; orcid.org/0000-0001-8347-0427; Email: Rebecca.Davie@kalvista.com

Authors

Hannah J. Edwards — KalVista Pharmaceuticals Limited, Salisbury SP4 0BF, U.K.

D. Michael Evans — KalVista Pharmaceuticals Limited, Salisbury SP4 0BF, U.K.

Simon T. Hodgson — KalVista Pharmaceuticals Limited, Salisbury SP4 0BF, U.K.

Michael J. Stocks — School of Pharmacy, University of Nottingham, Nottingham NG7 2RD, U.K.; orcid.org/0000-0003-3046-137X

Alun J. Smith — Sygnature Discovery, Nottingham NG1 1GR, U.K.

Louise J. Rushbrooke — KalVista Pharmaceuticals Limited, Salisbury SP4 0BF, U.K.

Stephen J. Pethen — KalVista Pharmaceuticals Limited, Salisbury SP4 0BF, U.K.

Michael B. Roe — KalVista Pharmaceuticals Limited, Salisbury SP4 0BF, U.K.; orcid.org/0000-0002-6858-1134

David E. Clark — Charles River Early Discovery, Harlow, Essex CM19 5TR, U.K.; orcid.org/0000-0002-3981-1893

Paul A. McEwan — Evotec, Abingdon OX14 4RZ, U.K.

Sally L. Hampton — KalVista Pharmaceuticals Limited, Salisbury SP4 0BF, U.K.

Complete contact information is available at:

<https://pubs.acs.org/10.1021/acs.jmedchem.2c00921>

Author Contributions

This manuscript was written through contributions of all authors. All authors have given approval to the final version of the manuscript.

Notes

The authors declare the following competing financial interest(s): RLD, HJE, DME, LJR, SJP, MBR, SLH are employees of KalVista Pharmaceuticals. STH and MJS were employees of KalVista Pharmaceuticals at the time of the study. DEC is an employee of Charles River, a company that was contracted by KalVista. PAM is an employee of Evotec, a company that was contracted by KalVista. AJS is an employee of Sygnature Discovery, a company that was contracted by KalVista.

■ ACKNOWLEDGMENTS

We thank David P. Rooker, Mitchell L. Childs, Sean Conroy, Stephen T. Hewison, and the Sygnature Discovery team (Colin Sambrook-Smith, Andrew Novak, Iain Miller, Ashvin Mistry, Giorgio Carbone, and Claire Cariou-Mumford) for their synthetic and medicinal chemistry analysis; Peter Robson and Josie L. Williams for the biology and ADME screening; and Natasha Bayliss for formulation and pharmacokinetic analysis.

■ ABBREVIATIONS USED

ADME, absorption, distribution, metabolism, and excretion; BK, bradykinin; C1-INH, C1 inhibitor; Caco-2, colon carcinoma cell line; CL_b, blood clearance; CL_{int}, intrinsic clearance; CL_p, plasma clearance; DXS, dextran sulfate; F, factor; FaSSGF, fasted state simulated gastric fluid; h, hours; HAE, hereditary angioedema; HATU, O-(7-azabenzotriazol-1-yl)-N,N,N',N'-tetramethyluronium hexafluorophosphate; HK, high-molecular-weight kininogen; HLM, human liver microsomes; KLK1, kallikrein-1; LBF, liver blood flow; LLE, lipophilic ligand efficiency; M, midazolam; MeOH, methanol; min, minutes; P1, P2, P3, P4 pockets, residues occupying substrate pockets; P_{app}, apparent permeability; PKa, plasma kallikrein; SAR, structure–activity relationship; S1, S2, S3, S4 pockets, substrate binding pockets; T, testosterone; V_{ss}, volume at steady state

■ REFERENCES

- (1) Cicardi, M.; Levy, R. J.; McNeil, D. L.; Li, H. H.; Sheffer, A. L.; Campion, M.; Horn, P. T.; Pullman, W. E. Ecallantide for the treatment of acute attacks in hereditary angioedema. *N. Engl. J. Med.* **2010**, *363*, S23–S31.
- (2) Kaplan, A. P. Enzymatic pathways in the pathogenesis of hereditary angioedema: the role of C1 inhibitor therapy. *J. Allergy Clin. Immunol.* **2010**, *126*, 918–925.
- (3) Zuraw, B. L.; Christiansen, S. C. HAE pathophysiology and underlying mechanisms. *Clin. Rev. Allergy Immunol.* **2016**, *51*, 216–229.
- (4) Lumry, W. R.; Settipane, R. A. Hereditary angioedema: epidemiology and burden of disease. *Allergy Asthma Proc.* **2020**, *41*, S08–S13.
- (5) Busse, P. J.; Christiansen, S. C.; Riedl, M. A.; Banerji, A.; Bernstein, J. A.; Castaldo, A. J.; Craig, T.; Davis-Lorton, M.; Frank, M. M.; Li, H. H.; Lumry, W. R.; Zuraw, B. L. US HAEA Medical Advisory Board 2020 guidelines for the management of hereditary angioedema. *J. Allergy Clin. Immunol. Pract.* **2021**, *9*, 132–150.

- (6) Sun, J. K.; Maturi, R. K.; Boyer, D. S.; Wells, J. A.; Gonzalez, V. H.; Tansley, R.; Hernandez, H.; Maetzel, A.; Feener, E. P.; Aiello, L. P. One-time intravitreal injection of KVD001, a plasma kallikrein inhibitor, in patients with central-involved diabetic macular edema and reduced vision: an open-label phase 1B study. *Ophthalmol. Retina* **2019**, *3*, 1107–1109.
- (7) Savitt, A. G.; Manimala, S.; White, T.; Fandaros, M.; Yin, W.; Duan, H.; Xu, X.; Geisbrecht, B. V.; Rubenstein, D. A.; Kaplan, A. P.; Peerschke, E. I.; Ghebrehwet, B. SARS-CoV-2 exacerbates COVID-19 pathology through activation of the complement and kinin systems. *Front. Immunol.* **2021**, *12*, 767347.
- (8) Schechter, I.; Berger, A. On the active site of proteases. *Biochem. Biophys. Res. Commun.* **1967**, *27*, 157–162.
- (9) Manallack, D. T.; Pranker, R. J.; Yuriev, E.; Oprea, T. I.; Chalmers, D. K. The significance of acid/base properties in drug discovery. *Chem. Soc. Rev.* **2013**, *42*, 485–496.
- (10) Xie, Z.; Li, Z.; Shao, Y.; Liao, C. Discovery and development of plasma kallikrein inhibitors for multiple diseases. *Eur. J. Med. Chem.* **2020**, *190*, 112137.
- (11) Riedl, M. A.; Ayyören-Pürsün, E.; Baker, J.; Farkas, H.; Anderson, J.; Bernstein, J. A.; Bouillet, L.; Busse, P.; Manning, M.; Magerl, M.; Gompels, M.; Huissoon, A. P.; Longhurst, H.; Lumry, W.; Ritchie, B.; Shapiro, R.; Soter, D.; Banerji, A.; Cancian, M.; Johnston, D. T.; Craig, T. J.; Launay, D.; Li, H. H.; Liebhauer, M.; Nickel, T.; Offenberger, J.; Rae, W.; Schrijvers, R.; Triggiani, M.; Wedner, H. J.; Dobo, S.; Cornpropst, M.; Clemons, D.; Fang, L.; Collis, P.; Sheridan, W. P.; Maurer, M. Evaluation of avoralstat, an oral kallikrein inhibitor, in a phase 3 hereditary angioedema prophylaxis trial: the OPuS-2 study. *Allergy* **2018**, *73*, 1871–1880.
- (12) Kotian, P. L.; Wu, M.; Vadlakonda, S.; Chintareddy, V.; Lu, P.; Juarez, L.; Kellogg-Yelder, D.; Chen, X.; Muppa, S.; Chambers-Wilson, R.; Parker, C. D.; Williams, J.; Polach, K. J.; Zhang, W.; Raman, K.; Babu, Y. S. Berotralstat (BCX7353): structure-guided design of a potent, selective, and oral plasma kallikrein inhibitor to prevent attacks of hereditary angioedema (HAE). *J. Med. Chem.* **2021**, *64*, 12453–12468.
- (13) McDonald, A.; Qian, S.; Kalfus, I. Treatment of hereditary angioedema. WO 2019/166874, September 6, 2019.
- (14) Kalfus, I.; Offman, E.; McDonald, A. Pharmacokinetics and safety of ATN-249, a novel oral plasma kallikrein inhibitor for hereditary angioedema. Presented at Western Society of Allergy, Asthma and Immunology (WSAAI, 2019), Maui, HI.
- (15) Chilcote, T. J.; Sinha, S. Inhibitors of plasma kallikrein. WO 2008/016883, February 7, 2007.
- (16) Chilcote, T. J.; Sinha, S. ASP-634: an oral drug candidate for diabetic macular edema. *Invest. Ophthalmol. Vis. Sci.* **2012**, *53* (14), 2240.
- (17) Nazaré, M.; Essrich, M.; Will, D. W.; Matter, H.; Ritter, K.; Urmann, M.; Bauer, A.; Schreuder, H.; Czech, J.; Lorenz, M.; Laux, V.; Wehner, V. Novel factor Xa inhibitors based on a 2-carboxyindole scaffold: SAR of P4 substituents in combination with a neutral P1 ligand. *Bioorg. Med. Chem. Lett.* **2004**, *14*, 4197–4201.
- (18) Flohr, S.; Markert, C.; Namoto, K.; Pirard, B. 5-Membered heteroarylcarboxamide derivatives as plasma kallikrein inhibitors. WO 2013/111108, August 1, 2013.
- (19) Corte, J. R.; Fang, T.; Pinto, D. J. P.; Han, W.; Hu, X.; Jiang, J.-X.; Li, Y.-L.; Gauuan, J. F.; Hadden, M.; Orton, D.; Rendina, A. R.; Luetgen, J. M.; Wong, P. C.; He, K.; Morin, P. E.; Chang, C.-H.; Cheney, D. L.; Knabb, R. M.; Wexler, R. R.; Lam, P. Y. S. Structure-activity relationships of anthranilamide-based factor Xa inhibitors containing piperidinone and pyridinone P4 moieties. *Bioorg. Med. Chem. Lett.* **2008**, *18*, 2845–2849.
- (20) Leeson, P. D.; Springthorpe, B. The influence of drug-like concepts on decision-making in medicinal chemistry. *Nat. Rev. Drug Discovery* **2007**, *6*, 881–890.
- (21) Irwin, J. J.; Shoichet, B. K. ZINC—a free database of commercially available compounds for virtual screening. *J. Chem. Inf. Model.* **2005**, *45*, 177–182.
- (22) Peters, S. A. Appendix I. In *Physiologically-Based Pharmacokinetic (PBPK) Modeling and Simulations: Principles, Methods, and Applications in the Pharmaceutical Industry*, 1st ed.; John Wiley & Sons: Hoboken, NJ, 2012; pp 407–421.
- (23) Duckworth, E. J.; Murugesan, N.; Li, L.; Rushbrooke, L. J.; Lee, D. K.; De Donatis, G. M.; Maetzel, A.; Yea, C. M.; Hampton, S. L.; Feener, E. P. Pharmacological suppression of the kallikrein kinin system with KVD900: an orally available plasma kallikrein inhibitor for the on-demand treatment of hereditary angioedema. *Clin. Exp. Allergy* **2022**, *52*, 1059–1070.
- (24) Tang, J.; Yu, C. L.; Williams, S. R.; Springman, E.; Jeffery, D.; Sprengeler, P. A.; Estevez, A.; Sampang, J.; et al. Expression, crystallization, and three-dimensional structure of the catalytic domain of human plasma kallikrein. *J. Biol. Chem.* **2005**, *280*, 41077–41089.
- (25) Li, Z.; Partridge, J.; Silva-Garcia, A.; Rademacher, P.; Betz, A.; Xu, Q.; Sham, H.; Hu, Y.; Shan, Y.; Liu, B.; Zhang, Y.; Shi, H.; Xu, Q.; Ma, X.; Zhang, L. Structure-guided design of novel, potent, and selective macrocyclic plasma kallikrein inhibitors. *ACS Med. Chem. Lett.* **2017**, *8*, 185–190.
- (26) Maetzel, A.; Smith, M. D.; Duckworth, E. J.; Hampton, S. L.; De Donatis, G. M.; Murugesan, N.; Rushbrooke, L. J.; Li, L.; Francombe, D.; Feener, E. P.; Yea, C. M. KVD900, an oral on-demand treatment for hereditary angioedema: phase 1 study results. *J. Allergy Clin. Immunol.* **2022**, *149*, 2034–2042.
- (27) LaPlante, S. R.; Bilodeau, F.; Aubry, N.; Gillard, J. R.; O'Meara, J.; Coulombe, R. N- versus O-alkylation: utilizing NMR methods to establish reliable primary determinations for drug discovery. *Bioorg. Med. Chem. Lett.* **2013**, *23*, 4663–4668.
- (28) Bolea, C.; Celanire, S.; Boudou, C.; Tang, L.; Rocher, J. P.; Liverton, N. J. Novel 2-amino-4-pyrazolyl-thiazole derivatives and their use as allosteric modulators of metabotropic glutamate receptors. WO 2012/009009, January 19, 2012.
- (29) Evans, D. M.; Davie, R. L.; Edwards, H. J.; Hodgson, S. T. N-((het)arylmethyl)heteroaryl-carboxamides compounds as plasma kallikrein inhibitors. 10,781,181, September 22, 2020.
- (30) Bernstein, J. M.; Li, H.; Yea, C.; et al. A022 On-demand oral treatment with KVD900 for HAE attacks achieves rapid exposure and improves patient outcomes. *Ann. Allergy Asthma Immunol.* **2021**, *127*, S4–S5.
- (31) Johansen, H. T.; Home, N. O.; Veggeland, T.; Briseid, K. Assay of kallikrein inhibitors and levels of acetone-activated kallikrein in plasma specimens from reactors to dextran or to contrast media. *Int. J. Tissue React.* **1986**, *8*, 185–192.
- (32) Shori, D. K.; Proctor, G. B.; Chao, J.; Ka-Ming, C.; Garrett, J. R. New specific assays for tonin and tissue kallikrein activities in rat submandibular glands: assays reveal differences in the effects of sympathetic and parasympathetic stimulation on proteinases in saliva. *Biochem. Pharmacol.* **1992**, *43*, 1209–1217.
- (33) Stürzebecher, J.; Prasa, D.; Sommerhoff, C. P. Inhibition of human mast cell tryptase by benzamidine derivatives. *Biol. Chem.* **1992**, *373*, 1025–1030.
- (34) Wang, Z.; Hop, C. E.; Leung, K. H.; Pang, J. Determination of in vitro permeability of drug candidates through a Caco-2 cell monolayer by liquid chromatography/tandem mass spectrometry. *J. Mass Spectrom.* **2000**, *35*, 71–76.
- (35) Obach, R. S. Prediction of human clearance of twenty-nine drugs from hepatic microsomal intrinsic clearance data: an examination of in vitro half-life approach and nonspecific binding to microsomes. *Drug Metab. Dispos.* **1999**, *27*, 1350–1359.
- (36) Obach, R. S.; Baxter, J. G.; Liston, T. E.; Silber, B. M.; Jones, B. C.; Macintyre, F.; Rance, D. J.; Wastall, P. The prediction of human pharmacokinetic parameters from preclinical and in vitro metabolism data. *J. Pharmacol. Exp. Ther.* **1997**, *283*, 46–58.
- (37) Lau, Y. Y.; Sapidou, E.; Cui, X.; White, R. E.; Cheng, K. C. Development of a novel in vitro model to predict hepatic clearance using fresh, cryopreserved, and sandwich-cultured hepatocytes. *Drug Metab. Dispos.* **2002**, *30*, 1446–1454.

- (38) *Biorelevant Media Preparation*, ver. 1.2, Biorelevant. http://www.biorelevant.com/site_upload_media/documents/Biorelevant_Media_Preparation_Instructions.pdf (accessed 2022-06-03).
- (39) Leigh, M.; Kloefer, B.; Schaich, M. Comparison of the solubility and dissolution of drugs in fasted-state biorelevant media (FaSSIF and FaSSIF-V2). *Dissolution Technol.* **2013**, *20*, 44–50.
- (40) Gabrielsson, J.; Weiner, D. Non-compartmental analysis. In *Pharmacokinetic and Pharmacodynamic Data Analysis: Concepts and Applications*, 4th ed.; Huang, X. H., Ed.; Swedish Pharmaceutical Press: Stockholm, 2007.